$Co_{1-x}Zn_xFe_2O_4$ nanofiber: Synthesized by electrospinning and its magnetic properties*

Dai Jian-Feng(戴剑锋)[a)b)†], Lu Rui-E(路瑞娥)[b)], Fu Bi(付 比)[c)], Gao Kun(高 锟)[d)], and Zhang Liang-Liang(张亮亮)[d)]

[a)] State Key Laboratory of Gansu Advanced Non Ferrous Metal Materials, Lanzhou 730050, China
[b)] School of Science, Lanzhou University of Technology, Lanzhou 730050, China
[c)] Frontier Institute of Science and Technology, Xi'an Jiaotong University, Xi'an 710000, China
[d)] State Key Laboratory for Manufacturing Engineering, Xi'an Jiaotong University, Xi'an 710000, China

(Received 31 May 2013; revised manuscript received 19 July 2013; published online 24 January 2014)

Well-aligned and uniform $Co_{0.8}Zn_{0.2}Fe_2O_4$ nanofibers (NFs) are prepared by electrospinning via sol–gel and subsequent heat treatment. Each of the as-spun NFs has a diameter of about 300 nm and a smooth surface morphology. The scanning electron microscope (SEM) image shows that the diameter decreases to 70 nm after the $Co_{0.8}Zn_{0.2}Fe_2O_4$ NF has been annealed at 650 °C for 3 h. The structure and chemical of $Co_{0.8}Zn_{0.2}Fe_2O_4$ NF are investigated by X-ray diffraction (XRD) and energy dispersive X-ray spectroscopy (EDS), respectively. Single phase cubic spinel structure, $Co_{0.8}Zn_{0.2}Fe_2O_4$ NF, is successfully obtained after having been calcined at 550 °C in air for 3 h, and a reduced lattice constant of the $Co_{0.8}Zn_{0.2}Fe_2O_4$ NF provides the evidence of effective Zn^{2+} substitution. The magnetic measurements show that the substitution of Zn^{2+} for Co^{2+} , i.e., the introduction of non-magnetic Zn^{2+} ions into A sites, can increase the saturation magnetization (M_s) and reduce the coercivity (H_c). The obtained H_c results of different samples reveal that the critical single-domain size of the $Co_{0.8}Zn_{0.2}Fe_2O_4$ NF is approximately 44 nm. By doping Zn^{2+} with different concentrations, the morphologies of $Co_{1-x}Zn_xFe_2O_4$ ($0 \le x \le 0.5$) NFs do not show obvious changes. For magnetic properties, the M_s increases and H_c decreases monotonically, respectively.

Keywords: alignment, $Co_{0.8}Zn_{0.2}Fe_2O_4$, single-domain, $Co_{1-x}Zn_xFe_2O_4$

PACS: 75.50.Gg, 75.75.Cd, 75.75.–c, 75.60.–d **DOI:** 10.1088/1674-1056/23/3/037505

1. Introduction

One-dimensional (1D) nanostructures of magnetic materials have attracted considerable scientific attention because of their unique properties and intriguing applications, such as mesoscopic physics, nanoscale devices, biological, medicine, heterostructures.[1–7] On a nanoscale, the interatomic exchange is no longer negligible compared with magnetostatic interactions, which leads to unique magnetic property.[8] There also have been a large number of techniques developed to fabricate 1D nanostructure with well-controlled morphology and chemical composition.[9–11] Among them, electrospinning was regarded as the simplest and most versatile technique for generating 1D nanostructure.[11] Because of the bending instability associated with the spinning technology jet, electrospun fibers are often deposited on the collector surface (a single piece of conductive substrate) as randomly oriented nonwoven mats, which could be unsatisfactorily dependent on some of their applications.[12] Oriented electrospun fibers can be prepared by using a rotating disk collector,[13] and such an aligned array can achieve higher levels of cell adhesion and proliferation by mimicking native bones.[10] The aligned fiber structures can also well control the porosity,[14] and improve the mechanical integrity[15] and unique electric and magnetic properties.[16]

Various types of materials including polymers, metal oxides, and hybrid (organic/inorganic) compounds, and some simple spinel ferrite nanofibers have been prepared via electrospinning.[17–19] On account of large magnetocrystalline anisotropy, high H_c, moderate M_s, higher T_c ($\sim$ 790 K),[20] and the highest value of absolute magnetostriction coefficient ($\lambda \sim 110 \times 10^{-6}$),[21] among the oxide based magnetostrictive materials, and the chemical and mechanical stability, cobalt ferrites are nowadays highly in demand. Moreover, Zn-substituted spinel-type ferrites are attractive because Zn substitution can change the magnetic and electric parameters in a wide range of values.[22] Substitution of low Zn^{2+} for Co^{2+} leads to the introduction of non magnetic Zn^{2+} ions into A sites, thus causing an increased magnetization. For higher Zn^{2+}doped $Co_{1-x}Zn_xFe_2O_4$, the M_s decreases with the increase of Zn^{2+} concentration, which can be explained on the basis of Yafet–Kittel type of spin arrangement.[23] Preparation and properties of Co–Zn ferrites have been reported. Wang and Li[24] investigated the properties of the nanosized $Co_{1-x}Zn_xFe_2O_4$ ($0 \le x \le 1.0$) nanoparticles, and found that

*Project supported by the National Natural Science Foundation of China (Grant No. 50873047) and the Foundation of Gansu Education Department, China (Grant No. 0603-02).

†Corresponding author. E-mail: daijf@lut.cn

© 2014 Chinese Physical Society and IOP Publishing Ltd

the M_s arrived at a highest value at $x = 0.4$. Characterizations of $Co_{1-x}Zn_xFe_2O_4$ nanoparticles synthesized by co-precipitation method indicated that the M_s reached a maximum at $x = 0.1$.[25] $Co_{1-x}Zn_xFe_2O_4$ NFs were prepared by electrospinning and found to have a critical concentration $x = 0.3$.[26] They also observed a decreasing behavior of saturation magnetization of the Co–Zn substituted ferrite nanoparticles with the increase of Zn concentration.[27,28]

In this study, we successfully prepare aligned $Co_{0.8}Zn_{0.2}Fe_2O_4$ NFs by improving the electrospinning setup with a rotating disk collector and find the critical single domain size of $Co_{0.8}Zn_{0.2}Fe_2O_4$ NF. Then based on previous reports, the effects of Zn^{2+} content on the magnetic properties of $Co_{1-x}Zn_xFe_2O_4$ ($0 \leq x \leq 0.5$) are characterized and discussed.

2. Experimental details

In a typical procedure, an appropriate amount of cobalt nitrate ($Co(NO_3)_2{\cdot}6H_2O$), zinc nitrate ($Zn(NO_3)_2{\cdot}6H_2O$), and ferric nitrate ($Fe(NO_3)_3{\cdot}9H_2O$) with $1-x:x:2$ molar ratios of Co:Zn:Fe was dissolved in N, N-Dimetylformamide (DMF), followed by magnetic stirring for 3 h to ensure the complete dissolution of the metal salt. Simultaneously, 0.45-g poly (vinyl pyrrolidone) (PVP, K30) was dissolved in ethanol (10 mL) and magnetically stirred for 3 h. Then 0.8-mL metal nitrates/DMF solution was added slowly into the PVP/ethanol solution under continuous stirring for 2 h and the blend served as the precursor. The obtained as-spun precursor solution was loaded into a plastic syringe with a stainless steel needle, which was connected to a high-voltage supply which could generate dc voltages of up to 50 kV. A rotating disc connected to the ground, with the distance between needle tip and the collector fixed at 15 cm, was used to collect the aligned fibers as described in a previous paper.[29] The rotating speed was fixed at 2000 rpm. The collected as-spun $Co_{1-x}Zn_xFe_2O_4$ NFs were dried at 50 °C for 5 h. The dried NFs were subsequently calcined at various temperatures for 3 h under an ambient atmosphere with a heating rate of 5 °C/min.

The crystalline structures of the annealed NFs were examined by X-ray diffraction (XRD, Netherlands PW3040) with Cu K_α radiation ($\lambda = 0.15418$ nm). The XRD samples were collected under electrospinning for several hours after having been annealed. The morphologies, diameters, and chemistries of NFs were examined by field emission scanning electron microscopy (FE-SEM, Hitachi S-4800), and the elemental analysis was performed by an energy dispersive Dispersive X-ray detector (EDX). All samples were sputter-coated with gold for 60 s prior to the observation with SEM. Ferromagnetic properties of the NFs were measured by a vibrating sample magnetometer (VSM, Lakeshore 7403, USA).

3. Results and discussion

3.1. X-Ray diffraction characterization

The XRD patterns of $Co_{0.8}Zn_{0.2}Fe_2O_4$ NFs after being calcined at different temperatures for 3 h are shown in Fig. 1. As observed, all peaks can be readily indexed to cubic spinel structure (JCPDS: #22-1086), which shows that there exists only a single phase: no phase transition of Zn-doped $Co_{0.8}Zn_{0.2}Fe_2O_4$ appears. The peaks of (111) and (422) are both very weak at 500 °C, because the cubic spinel phase cannot completely form at low temperature. After calcination at higher temperatures (550 °C–950 °C), a well-developed spinel structure is successfully obtained, and no other phases are detected on these samples. Besides, with calcination temperature increasing from 550 °C to 950 °C, the main features of XRD patterns did not change, except for the sharpening of the reflection peaks, but the peak positions shift toward low angle for the (311) peak as shown in the enlarged portion of the pattern in Fig. 1(b). This lower angle shift corresponds to the increase of the lattice constants owing to lattice expansion during the heat treatment process, which is summarized in Table 1. The observed evolution of narrower peaks reveals the increase in crystallite size and crystallinity in the calcination process. The average crystallite size (D) can be calculated from the value of full-width at half-maximum (FWHM) of the prominent (311) reflection using Scherrer's equation ($D = 0.89\lambda/\beta\cos\theta$), and the calculated results of all samples are listed in Table 1. It can be seen from Table 1 that the crystallite size increases from 17.0 nm to 61.9 nm for the sample calcined at 550 °C–950 °C.

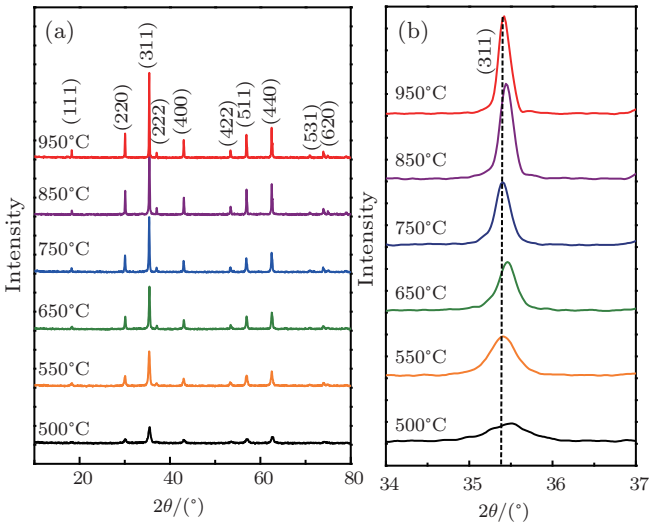


Fig. 1. (color online) (a) XRD patterns of $Co_{0.8}Zn_{0.2}Fe_2O_4$ composite fibers calcined at various temperatures in air for 3 h, (b) (311) peaks show the lower angle for higher temperatures of Zn-doped $Co_{0.8}Zn_{0.2}Fe_2O_4$ NFs.

Table 1. X-ray diffraction studies and magnetic parameters of $Co_{0.8}Zn_{0.2}Fe_2O_4$ NFs calcined in air for 3 h at various temperatures (1 Oe = 79.5775 A/m, 1 Å = 10^{-10}m).

$Co_{0.8}Zn_{0.2}Fe_2O_4$ NFs	Lattice parameter/Å	Mean grain size/nm	Magnetization /emu·g^{-1}	Coercivity /Oe	Remanent magnetization/emu·g^{-1}	Squareness ratio M_r/M_s
500 °C	8.3925	17.0	–	–		–
550 °C	8.3961	20.5	16.6	314.3	5.3	0.336
650 °C	8.3973	35.3	46.7	363.9	16.9	0.326
750 °C	8.3983	44.2	66.1	525.7	19.9	0.302
850 °C	8.3996	56.5	75.4	494.1	26.7	0.355
950 °C	8.4021	61.9	87.2	446.4	34.1	0.391

The XRD patterns of non-doped and doped NFs are compared in Fig. 2. The XRD patterns of the Zn-doped shift by a higher angle ($\Delta(2\theta) = 0.20°$) for the (311) peak, which means that the lattice parameters are slightly smaller than those of $CoFe_2O_4$ obtained in our experiment and those of $CoFe_2O_4$ ($a = 8.3919$ Å) reported in the standard data card (JCPDS:22-1086). This can be predominantly attributed to the replacement of larger Co^{2+} ions (0.65 Å)[30] by smaller Zn^{2+} ions (0.60 Å).[31]

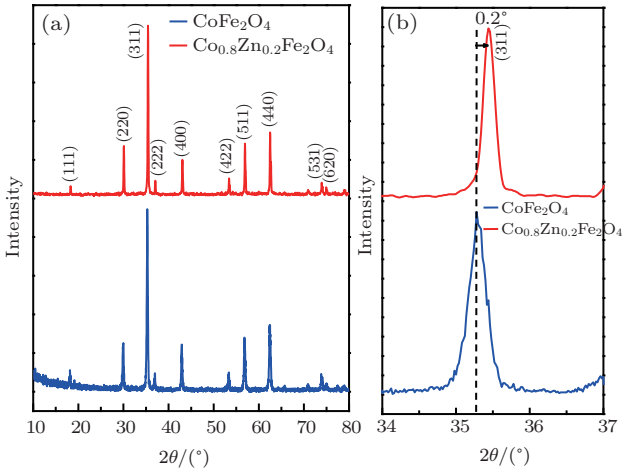


Fig. 2. (color online) (a) XRD patterns of $Co_{0.8}Zn_{0.2}Fe_2O_4$/$CoFe_2O_4$ NFs calcined at 850 °C in air for 3 h, (b) (311) peaks show the higher angle for the $Co_{0.8}Zn_{0.2}Fe_2O_4$ NFs.

3.2. The morphology of $Co_{1-x}Zn_xFe_2O_4$ NFs

As is well known, the morphology of electrospun fibers is dependent on several parameters,[21] such as viscosity and electroconductibility of the solution, electric intensity, collection distance, and rotating speed of the disc. Among these parameters, viscosity of solution and speed of disc are the two most important parameters for obtaining the aligned fibers. By controlling the appropriate solution for electrospinning, aligned fibers are collected at a disc rotating speed of 2000 rpm. Figures 3(a)–3(d) show the SEM images of aligned NFs calcined at various temperatures for 3 h; it can be seen that as-spun $Co_{0.8}Zn_{0.2}Fe_2O_4$ fiber surfaces are smooth due to their amorphous nature and most of them are straight and uniform each with a diameter of 300 nm (Fig. 3(a)). After being calcined at 550 °C (Fig. 3(b)), the diameters of fibers shrink to 100 nm and the surfaces become rough due to the small grains, which can be confirmed by XRD patterns where the crystallization of $Co_{0.8}Zn_{0.2}Fe_2O_4$ NFs begins to occur at this temperature. The surfaces of the NFs become porous and the diameters decrease to 70 nm with temperature further increasing to 650 °C (Fig. 3(c)). At the high temperature, there is no apparent change in diameter and the porous fibers disappear. Large particles are formed on the surfaces of these fibers when the temperature is increased to 850 °C due to grain growth of nanocrystalline $Co_{0.8}Zn_{0.2}Fe_2O_4$. At this temperature, the fibers become curved and lead to the reduction of orientation degree and the morphologies of the calcined fibers each gradually transform from a porous structure to a necklace-like nanostructure (Fig. 3(d)). This can be attributed to the fact that some small irregular particles agglomerate, and form large size ones.[32] As is well known, the magnetic property is closely related to particle size and morphology. For example, the hollow cobalt nanochain composite has negative permeability.[33]

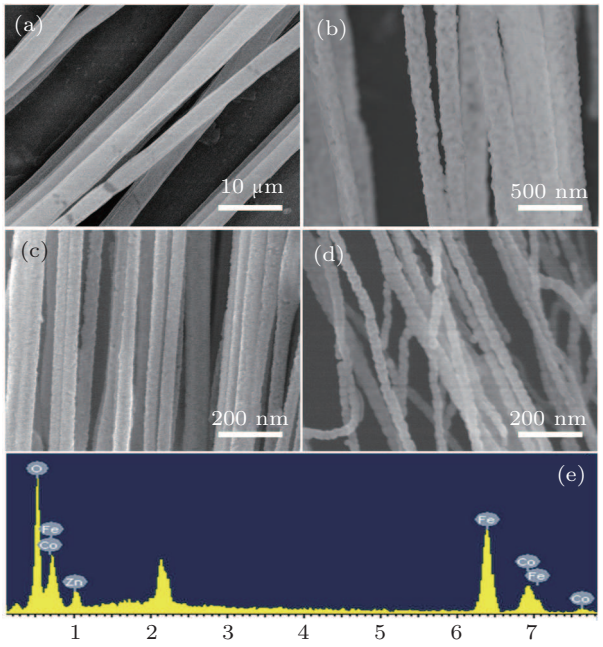


Fig. 3. (color online) SEM images of aligned $Co_{0.8}Zn_{0.2}Fe_2O_4$ NFs calcined at various temperatures for 3 h in air and EDS spectrum: (a)–(d) SEM images of as-spun, 550 °C, 650 °C, 850 °C, respectively; (e) EDS spectrum of $Co_{0.8}Zn_{0.2}Fe_2O_4$ NFs.

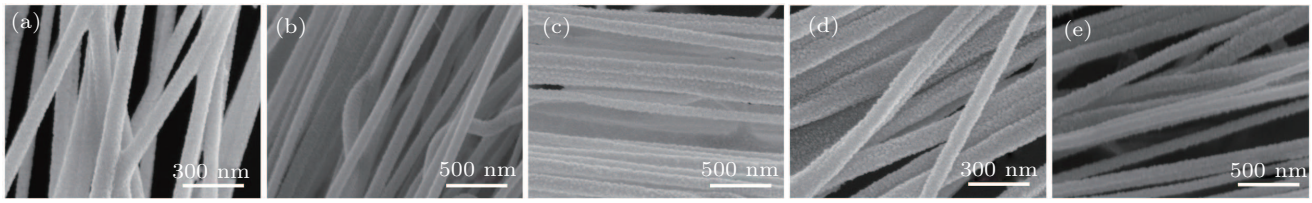


Fig. 4. SEM images of $Co_{1-x}Zn_xFe_2O_4$ NFs calcined in air at 800 °C for 1 h: (a) $x = 0$, (b) $x = 0.2$, (c) $x = 0.3$, (d) $x = 0.4$, (e) $x = 0.5$.

Figure 3(e) displays the EDX spot scanning spectrum of Fe, Co, Zn, and O elements, their concentrations are estimated to be 47.89%, 33.86%, 13.67%, and 4.58%, respectively. The EDS result is consistent with the molar ratio [Fe]/[Co]/[Zn]/[O] in $Co_{0.8}Zn_{0.2}Fe_2O_4$, and indicates the effective Zn substitution, which is also confirmed by the lattice constant calculation results from XRD.

Figure 4 shows the SEM images of $Co_{1-x}Zn_xFe_2O_4$ NFs with different Zn content values, calcined at 800 °C for 1 h in air. The surfaces of $Co_{1-x}Zn_xFe_2O_4$ NFs are relatively rough, owing to the crystallization. When Zn content increases, both the diameters and the surfaces of all samples have no apparent changes and the mean diameter of NFs is about 100 nm.

3.3. Magnetic measurements

Room-temperature magnetic hysteresis loops for $Co_{0.8}Zn_{0.2}Fe_2O_4$ NFs calcined at various temperatures in air for 3h are shown in Fig. 5. These hysteresis loops are typical curves of ferromagnetism and the saturation magnetization, and the values of coercivity and squareness ratio (M_r/M_s) of all samples, derived from the hysteresis measurements, are presented in Table 1. From Table 1, the values of specific saturation magnetization (M_s) increase with the increases of calcine temperature and grain size. This should be attributed to the weakening of the non-collinearity induced by finite-size and surface effects, which can lead to a reduction in the proportion of the surface-spin magnetic moment as $Co_{0.8}Zn_{0.2}Fe_2O_4$ crystalline proceeds.[34] In addition, the enhancements of purity and crystallinity of NFs may also be important reasons for this. It is noted that the M_s values obtained from the 750 °C samples (each with a crystallite size of $\sim$ 44.2 nm, 66.1 emu/g) are comparable to the reported value of 61.9 emu/g for the $CoFe_2O_4$ NF with a crystallite size of $\sim$ 54 nm prepared by electrospinning.[35]

Figure 5(b) shows the curves of M_s and H_c versus grain size for $Co_{0.8}Zn_{0.2}Fe_2O_4$ NF. Corresponding to the increase of temperature and nanocrystal growth process, the value of H_c increases initially and then reaches a maximum value at a grain size of 44.2 nm (at 750 °C). Afterwards, it begins to decrease with the further increase of crystallite size. This can be explained by the magnetization reversal mechanism of the grains, and the coercivity in the single domain region is expressed as $H_c = g - h/D^2$. In the multi domain region the variation of coercivity with grain size can be expressed as $H_c = a + b/D$, where g, h, a, and b are constants and D is the grain diameter.[36] Hence, in the multi domain region the coercivity decreases as grain diameter increases. The studies of crystallite-size-dependent coercivity reveal that the single-domain size of the $Co_{0.8}Zn_{0.2}Fe_2O_4$ NF is about 44 nm, which is close to $CoFe_2O_4$ single-domain size 40 nm as reported in Ref. [19].

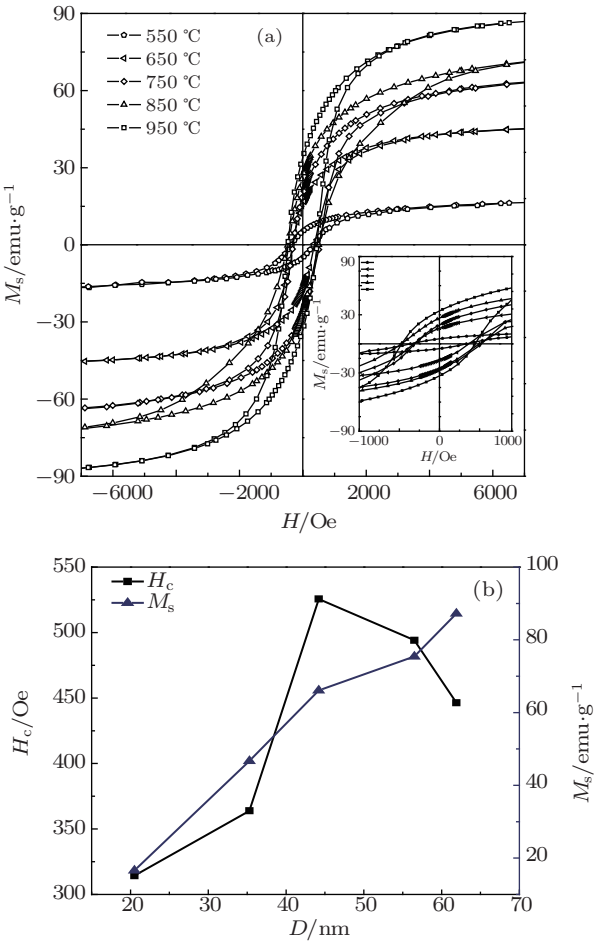


Fig. 5. Room temperature hysteresis loops for (a) $Co_{0.8}Zn_{0.2}Fe_2O_4$ NFs calcined at various temperatures in air for 3 h (the inset shows the curves of enlarged partial hysteresis and coercivity in detail), (b) Variations of the saturation magnetization (M_s) and coercivity (H_c) with temperature for $Co_{0.8}Zn_{0.2}Fe_2O_4$ NFs.

We also investigate the effect of Zn content on the magnetic property of cobalt-zinc ferrite. Figure 6(a) shows the room-temperature hysteresis loops for $Co_{1-x}Zn_xFe_2O_4$ ($0 \leq x \leq 0.5$) NFs, calculated at 650 °C in air for 3 h. Figure 6(b) reveals that the values of M_s and H_c of $Co_{1-x}Zn_xFe_2O_4$ increase

and decrease monotonically with the increase of Zn content, respectively. The change in magnetic property such as M_s and H_c is due to the influence of the cationic stoichiometry and occupancy at the specific sites. As is well known, Zn^{2+} ions occupy the tetrahedral A sites while Co^{2+} ions tend to occupy the octahedral B sites. The substitution of non-magnetic Zn^{2+} ions for magnetic Co^{2+} ions will change the distribution of cations and move magnetic Fe^{3+} ions from A sites to B sites, resulting in the increase of net magnetic moment per formula unit due to the prominent inter-sublattice A–B super-exchange interaction at low Zn^{2+} content.[26] On the contrary, for higher Zn-doped $Co_{1-x}Zn_xFe_2O_4$, the M_s decreases with the increase of Zn concentration,[22,24–26] which can be explained on the basis of Yafet–Kittel type of spin arrangement.[23] In our results, the M_s increases with the increase of Zn concentration ($0 \leq x \leq 0.5$), indicating that the concentration of Zn ions in the experiment has not reached the highest doping point of $Co_{1-x}Zn_xFe_2O_4$ NFs. In terms of the single ion model of magnetic anisotropy,[37] the replacement of Co^{2+} ions by Zn^{2+} ions will cause the decrease of magnetocrystalline anisotropy, and consequently will result in the reduction of coercivity of $Co_{1-x}Zn_xFe_2O_4$ NFs.

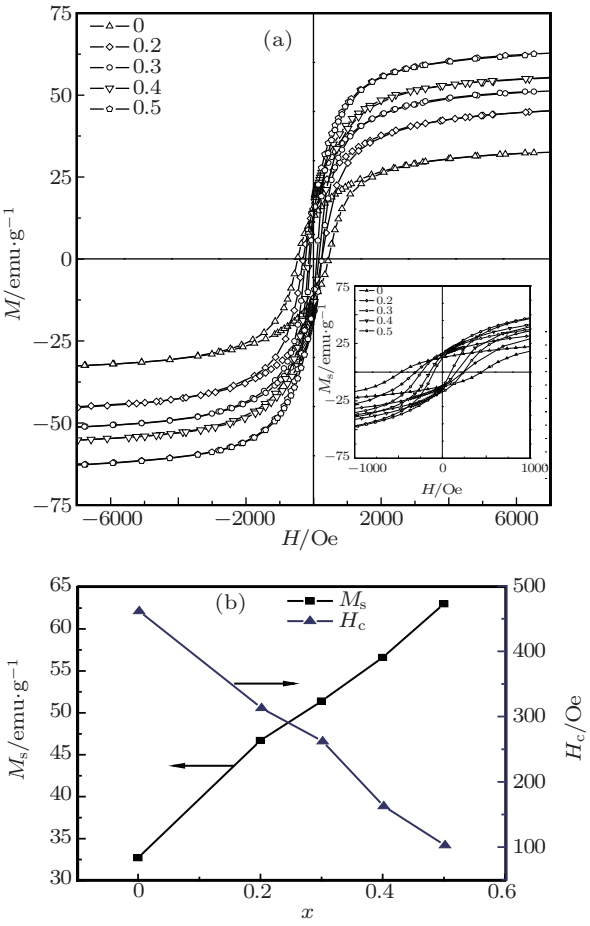


Fig. 6. Room-temperature hysteresis loops for $Co_{1-x}Zn_xFe_2O_4$ ($x = 0$–0.5) NFs calcined at 650 °C in air for 3 h and the enlarged partial hysteresis curves (in the inset) (a), and the variations of M_s and H_c of $Co_{1-x}Zn_xFe_2O_4$ with Zn concentration (b).

4. Conclusions

In this paper, the aligned and uniform as-spun composite NFs with ~ 300 nm in diameter are prepared by sol–gel assisted electrospinning technique. The $Co_{0.8}Zn_{0.2}Fe_2O_4$ NFs have a pure cubic spinel structure after the as-spun composite has been calcined at 550 °C–950 °C in air for 3 h, which is confirmed by XRD analysis. The lattice constant increases with the calcination temperature increasing but decreases as Zn atoms are doped. The morphologies and diameters of NFs are largely affected by calcine temperature. With the temperature increasing to 850 °C, the morphologies of the calcined NFs gradually change from a porous structure to a necklace-like structure. The room temperature magnetic hysteresis loops for all calcined samples of $Co_{0.8}Zn_{0.2}Fe_2O_4$ NFs each exhibit ferromagnetism. The value of M_s is found to increase with crystal size, owing to finite-size and surface effects, while the value of H_c first increases and then decreases with the increase of crystal size. The H_c dependence on grain size reveals that the single-domain size of the $Co_{0.8}Zn_{0.2}Fe_2O_4$ NF is about 44 nm. The surfaces of $Co_{1-x}Zn_xFe_2O_4$ ($0 \leq x \leq 0.5$) NFs do not show much change, while the magnetic properties, that is, the M_s and H_c are found to increase and decrease monotonically with zinc concentration, respectively.

References

[1] Xia Y N, Yang P D, Sun Y G, Wu Y Y, Brian M, Byron G, Yin Y D, Kim F and Yan H Q 2003 *Adv. Mater.* **15** 353
[2] Neuberger T, Schopf B, Hofmann H, Hofmann M and Rechenberg B V 2005 *J. Magn. Magn. Mater.* **293** 483
[3] Sawhney A P S, Condon B, Singh K V, Pang S S, Li G and David H 2008 *Text. Res. J.* **78** 731
[4] Kou X, Fan X, Zhu H and Xiao Q 2009 *J. Appl. Phys. Lett.* **94** 112509
[5] Hu J T, Wang T, Charles M and Lieber 1999 *Acc. Chem. Res.* **32** 435
[6] Kang Y Q, Cao M S, Yuan J, Zhang L, Wen B and Fang X Y 2010 *J. Alloys Compd.* **495** 254
[7] Cao M S, Yang J, Song W L, Zhang D Q, Wen B, Jin H B, Hou Z L and Yuan J 2012 *ACS Appl. Mater. Interfaces* **4** 6949
[8] Skomski R 2003 *J. Phys.: Condens. Matter* **15** 841
[9] Gong J F, Dou Z M, Wang Z Q, Zhang B, Zhu W H, Zhang K X, Liu M Y, Zhu H and Zhou J F 2012 *Chin. Phys. B* **21** 068101
[10] Bai A Q, Zheng J, Tao Y L, Zuo Y H, Xue C L, Cheng B W and Wang Q M 2011 *Chin. Phys. B* **20** 116103
[11] Ersen O, Begin S, Houlle M, Amadou J, Janowska I, Greneche J M, Crucifix C and Huu C P 2008 *Nano Lett.* **8** 1033
[12] Li D, Amit B, Samson A, Jenekhe and Xia Y N 2004 *Adv. Mater.* **16** 2062
[13] Theron A, Zussman E and Yarin A L 2001 *Nanotechnology* **12** 384
[14] Zhu X L, Cui W G, Li X H and Jin Y 2008 *Biomacromolecules* **9** 1795
[15] Matthews J A, Wnek G E and Simpson D G 2002 *Biomacromolecules* **3** 232
[16] Qing K Y, Sheng C M, Jie Y and Yong F X 2010 *Chin. Phys. B* **19** 017701
[17] Li D and Xia Y N. 2004 *Adv. Mater.* **16** 1151
[18] Sanchez A M, Åkäslompol L, Qin Q H and Dijken S 2012 *Cryst. Growth Des.* **12** 954
[19] Li D, Herricks T and Xia Y N 2003 *Appl. Phys. Lett.* **83** 4586
[20] Ponhan W and Maensiri S 2009 *Solid State Sci.* **11** 479
[21] Gupta A, Shannigrahi H S and Chatterjee R 2011 *Appl. Phys. Lett.* **98** 112901
[22] Arulmurugan G, Vaidyanathan S and Sendhilnathan B 2005 *Physica B* **368** 223

[23] Yafet Y and Kittel C 1952 *Phys. Rev.* **87** 290
[24] Wang L and Li F S 2008 *Chin. Phys. B* **17** 1858
[25] Vaidyanathana G and Sendhilnathan S 2008 *Physica B* **403** 2157
[26] Shen X Q, Xiang J, Song F Z and Liu M Q 2010 *Appl. Phys. A* **99** 189
[27] Islam M U, Rana M U and Abbbas T 1998 *Mater. Chem. Phys.* **57** 190
[28] Vaidyanathan G, Sendhilnathan S and Arulmurgan R 2008 *J. Magn. Magn. Mater.* **320** 803
[29] Dai J F, Wang J H, Mu X W and Chen X T 2011 *J. Reinf. Plast. Compos.* **30** 1179
[30] Chawla S K, Mudsainiyan R K, Meena S S, Yusuf S M and Singh N 2011 *AIP Conf. Proc.* **1447** 1243
[31] Belghazi Y, Schmerber G, Colis S, Rehspringer J L, Berrada A and Dinia A 2007 *J. Magn. Magn. Mater.* **301** 2092
[32] Lu R, Yuan J, Shi H L, Li B, Wang W Z, Wang D W and Cao M S 2013 *Cryst. Eng. Commun.* **15** 3984
[33] Shi X L, Cao M S, Yuan J and Fang X Y 2009 *Appl. Phys. Lett.* **95** 163108
[34] Raghavender A T, Pajic D, Zadro K, Milekovic T, Rao P V, Jadhav K M and Ravinder D 2007 *J. Magn. Magn. Mater.* **316** 1
[35] Montana S and Santi M 2009 *Appl. Phys. A* **97** 167
[36] George M, John A M, Nair S S, Joy P A and Anantharaman M R 2006 *J. Magn. Magn. Mater* **302** 190
[37] Salazar-Alvarez G, Olsson R T, Sort J, Macedo W A A, Ardisson J D, Baró M D, Gedde U W and Nogués J 2007 *Chem. Mater.* **19** 4957